New vesicular carbon-based rhenium phosphides with all-pH range electrocatalytic hydrogen evolution activity

Fang Sun[a], Yanwei Wang[a], Ling Fang[a], Xiaohui Yang[a], Weiwei Fu[a], Danning Tian[c], Zhengyong Huang[b], Jian Li[b], Huijuan Zhang[a], Yu Wang[a,b,*]

[a] The School of Chemistry and Chemical Engineering, State Key Laboratory of Power Transmission Equipment & System Security and New Technology, Chongqing University, 174 Shazheng Street, Shapingba District, Chongqing City, 400044, PR China
[b] The School of Electrical Engineering, Chongqing University, 174 Shazheng Street, Shapingba District, Chongqing City 400044, PR China
[c] High School Affiliated to Southwest University, Chongqing City, 400700, PR China

ARTICLE INFO

ABSTRACT

Considering the great application prospect of noble metal rhenium (Re) in the catalytic field derived from its intrinsic properties, exploring more novel and highly effective Re-based catalysts becomes an important topic. Herein, for the first time, we design a novel strategy for fabrication of Re_2P and Re_3P_4 nanoparticles anchored in N, P doped vesicular carbon (NPVC) via pyrolyzing ammonium perrhenate (NH_4ReO_4), 1-hydroxyethylidene-1,1-diphosphonic acid (HEDP) and melamine on the surface of SiO_2 spheres. Choosing hydrogen evolution as a probe reaction, Re_3P_4@NPVC heterostructure exhibits highly efficient catalytic activity compared with as-synthesized samples, which rivals the commercial Pt/C. Concretely, the Tafel slope is 38, 77 and 62 mV dec^{-1}, and overpotential is 40, 70 and 61 mV at 10 mA cm^{-2} in 0.5 M H_2SO_4, 1 M phosphate buffer solution and 1 M KOH, respectively. Both experiment and DFT calculation unambiguously validate that Coupling metal Re and P is able to promote the HER pathway by tuning the ΔG_{H*} value close to the optimum, balancing adsorption and desorption of hydrogen. Besides, the electronic coupling of NPVC layer and NPs synergistically enhances the proton adsorption and reduction kinetics.

1. Introduction

Demand for energy is higher than ever because of the increasing global population density, the growing climate change and environmental issues [1]. Hydrogen, as the ideal clean green and high calorific value energy, has long been considered to have the greatest potential to replace fossil fuels [2]. Up to now, the electrochemical water splitting is believed as an attractive strategy to effectively generate hydrogen with high yield and excellent purity [3]. Hydrogen evolution reaction (HER), as a fundamental step of electrochemical water splitting, is being acclaimed as a cornerstone for exploring other multi-electron transfer process mechanisms in electrocatalysis [4]. In practical applications, achieving rapid kinetics for HER always requires favourable catalysts. Noble metals have received considerable attention because of their huge potential in the field of environmental and industrial catalysis research [5]. Among them, noble metal rhenium (Re) has attracted researchers due to its exceptional plasticity, mechanical, creep resistance, good wear and corrosion resistance [6]. In particular, Re

usually displays excellent catalytic activity, which play pivotal role in petrochemical engineering [7], ammonia synthesis [8], and photoelectrocatalysis [9], hydrodesulfurization (HDS) [10], hydrodenitrogenation (HDN) [11]. Re has been developed as an electrocatalyst for HER [12], and has shown unusual electrocatalytic activities. Impressively, the exchange density current (j_O) on Re ($j_O = 1.35$ mA cm^{-2}) is higher than the value of Pt ($j_O = 0.79$ mA cm^{-2}) in acidic solution [13], Moreover, Miles determined that the performance of Re was considered to perform similarly as Co, Rh, Fe, Ir and Ni in parallel research in alkaline media [14]. Unfortunately, the extensive application with rhenium catalyst is hindered for its fancy price, complex natural extraction and rarity [6]. As a consequence, it is necessary and meaningful to develop more novel and high-efficiency Re-based catalyst materials with low metal loading [12,15].

A typically eye-attracting research is transition metal phosphides (TMPs) catalysts design for HER due to their wide range of compositions and tuning the electronic structure, especially the advent of iron phosphides, nickel phosphides and cobalt phosphides as highly efficient

---

HER electrocatalysts [1,16]. Many previous studies have certified that introducing phosphorus (P) incorporated into the lattice of the transition metal can significantly improve the electrocatalytic performances due to the capability of effectively accommodating the electronic structure [17]. Consequently we wondered to know whether rhenium phosphide can possess remarkable catalytic properties based on the influence of P on the electronic state of metal elements, thus regulating the free energy of H* adsorption (ΔG_{H*}) and making it a high-efficiency electrocatalyst for HER. In general, there are many kinds of alternative P sources to obtain transition metal phosphides (TMPs), such as red phosphorus, hypophosphites, tri-*n*-octylphosphine and tri-phenylphosphine. However, They're either flammable and corrosive dangerous reagents, or they release toxic products during the synthesis process [18,19]. Accordingly, seeking new, eco-friendly and secure phosphorus sources for fabrication TMPs becomes an important topic. The 1-hydroxyethylidene-1,1-diphosphonic acid (HEDP) molecule containing two phosphate groups not only can act as a P source but also chelate the metallic ions [20]. Therefore, it has been widely used in various fields (water treatment agent, cosmetic component, and corrosion inhibitor), and is considered as a biosafety material [21]. Additionally, using one-pot pyrolysis to construct heteroatom doped carbon substrate can enhance corrosion tolerance and conductivity of the electrocatalysts, thus synergistically boosting the catalytic process toward HER [22,23]. Nevertheless, in these cases, it would lead to the agglomeration of the carbon support, causing the uneven dispersion or big size of nanoparticles.

Here inspired by these facts, for the first time, small-size Re_2P and Re_3P_4 (ca. 4 nm) inlaid in thinner N,P dual doped vesicular carbon (denoted as $Re_2P@NPVC$ and $Re_3P_4@NPVC$, respectively) are designed by using HEDP as the P source. In contrast with the $Re@NPVC$, we find that phosphides are more favourable to the HER at all-pH range. The $Re_3P_4@NPVC$ behave as ultraefficient HER electrocatalysts with overpotentials 40, 70 and 61 mV at a fixed current density (10 mA cm^{-2}) in 0.5 M H_2SO_4, 1 M phosphate buffer solution and 1 M KOH, respectively, and corresponding Tafel slopes of is 38, 77 and 62 mV dec^{-1}, which are comparable with Pt/C. Density functional theory (DFT) calculations also unmask that introducing P element into the crystal lattice of Re can achieve the excellent HER performance. Moreover, DFT calculations also prove that the electronic coupling not only enhances the conductivity of catalyst but also provides efficient routes for electron transfer for HER.

2. Experimental section

2.1. Preparation of SiO₂ template

According to the classical stöber method [24], absolute ethanol (60 mL), deionized (DI) water (20 mL), and 28% ammonia solution (2.8 mL) were orderly added into a 200 ml beaker under robust stirring, then tetraethyl orthosilicate (TEOS) (2.4 mL) being quickly added into the mixture under agitation. The white precipitate was seen for a reaction time 10 h. Finally, the as-synthesized SiO₂ spheres were obtained after being washed at least three cycles of centrifugation with DI and anhydrous ethanol and being placed in a vacuum box at 60 ℃ overnight.

2.2. Preparation of Re₃P₄@NPVC, Re₂P@NPVC, Re@NPVC, NPVC and Re₃P₄@NPC

Ammonium perrhenate (NH₄ReO₄) (15 mg), HEDP (1 mL) and melamine (50 mg) were dissolved in a 30 mL aqueous ethanol solution (volume ratio of 7:3). After stirring for 20 min, the prepared SiO₂ was added into the mixed solution under robust stirring. Then, the solution was heated to 85 ℃ under stirring by an oil bath until drying it up. The solid mixture was then annealed (880 ℃, 2 h) under inert gas environment. After cooled down to room temperature, the **black** product

was added into HF solution to etch the SiO₂. The precipitate at the bottom was repeatedly washed with DI and anhydrous ethanol to remove the residue of reactants. Finally, the black powder of Re₃P₄@NPVC was obtained by drying in a vacuum at 60 ℃ overnight. Without changing other synthetic conditions, Re₂P@NPVC was obtained by decreasing the quantity HEDP to 375 μL. When the annealing temperature was 650 ℃ for 2 h under inert atmosphere, Re@NPVC can be obtained via the same steps as Re₃P₄@NPVC. NPVC was prepared via the same steps as Re₃P₄@NPVC without adding NH₄ReO₄. Re₃P₄@NPC was also made via the same steps as Re₃P₄@NPVC without etching the SiO₂ template with HF solution.

2.3. Preparation of Re₃P₄ bulk

The NH₄ReO₄ was placed at the central position of a closed graphite boat, and red phosphorus was placed at the upstream side of the furnace (the weight ration of NH₄ReO₄ and red phosphorus is about 1:3). Subsequently, Re₃P₄ bulk was obtained after being annealed (880 ℃, 2 h) under inert atmosphere.

2.4. Materials characterization

The microscopic morphologies and structures of our materials were characterized field emission scanning electron microscopy (SEM, JEOL, JSM-7800 F, 15 kV), transmission electron microscopy (TEM, JEOL, JEM-2100, FEI Talos F200X and FEI Titan Cubed Themis G2 300 with a probe corrector) that is coupled with EDX analysis. The chemical components and surface chemical states of our materials were evaluated by powder X-ray diffraction (XRD, PANalytical X'Pert Powder with Cu Ka radiation) and X-ray photo electron spectrometer (XPS) with an ESCA-LAB250 analyzer from Thermo scientific using monochromatic Al Kα radiation (225 W, 15 mA, 15 kV). Besides, Brunauer-Emmett-Teller surface area measurement (BET, Quantachrome Autosorb-6B surface area and Pore size analyzer), inductively coupled plasma atomic emission spectroscopy (ICP-AES, Thermo iCAP 6300Duo) and Raman Microscopy (RENISHAW Invia, 100–240 V, 150 W) were also necessary means of characterization.

2.5. Electrochemical measurements

All HER properties were investigated in a three-electrode device (glassy carbon electrode (GCE), carbon rod and saturated calomel electrode (SCE)) using CHI 760E electrochemical work station (CH Instruments, Inc., Shanghai). The GCE, a carbon rod and SCE act as working electrode, counter electrode and reference electrode in acidic (0.5 M H_2SO_4) and neutral (1.0 M PBS), respectively. The alkaline (1.0 M KOH) electrochemical measurements were performed using Hg/HgO as the reference electrode. 2 mg sample was evenly dispersed in a mixture composed of Nafion solution (0.5 wt%, 100 μL) and ethanol (300 μL) by ultrasonication (30 min). Subsequently, the 2 μL obtained ink was dried on the GC electrode to prepare working electrode with loading amount of 0.143 mg cm^{-2}. And all of the potential (E(SCE)) in this work was transferred into E(RHE) using the formula:

$$E_{RHE} = E_{SCE} + 0.059 \, pH + E_{SCE}^0$$

Besides, we prepared various samples acted as working electrodes for comparison, respectively. The linear sweep voltammetry were executed to obtain the polarization profiles and Tafel slopes at a scan rate of 5 mV s^{-1} in different pH conditions (0.5 M H_2SO_4, 1 M KOH, and 1.0 M PBS). Under the potentiostatic condition when the frequency range is from 10,000 to 0.1 Hz, the Nyquist plots of electrochemical impedance spectroscopy (EIS) were gained with the amplitude of 10 mV. From the measurement of cyclic voltammetry in the voltage range of 0.00-0.10 V (vs RHE), the electrochemical active surface areas (ECSA) were obtained in 0.5 M H_2SO_4 solution. For overall water
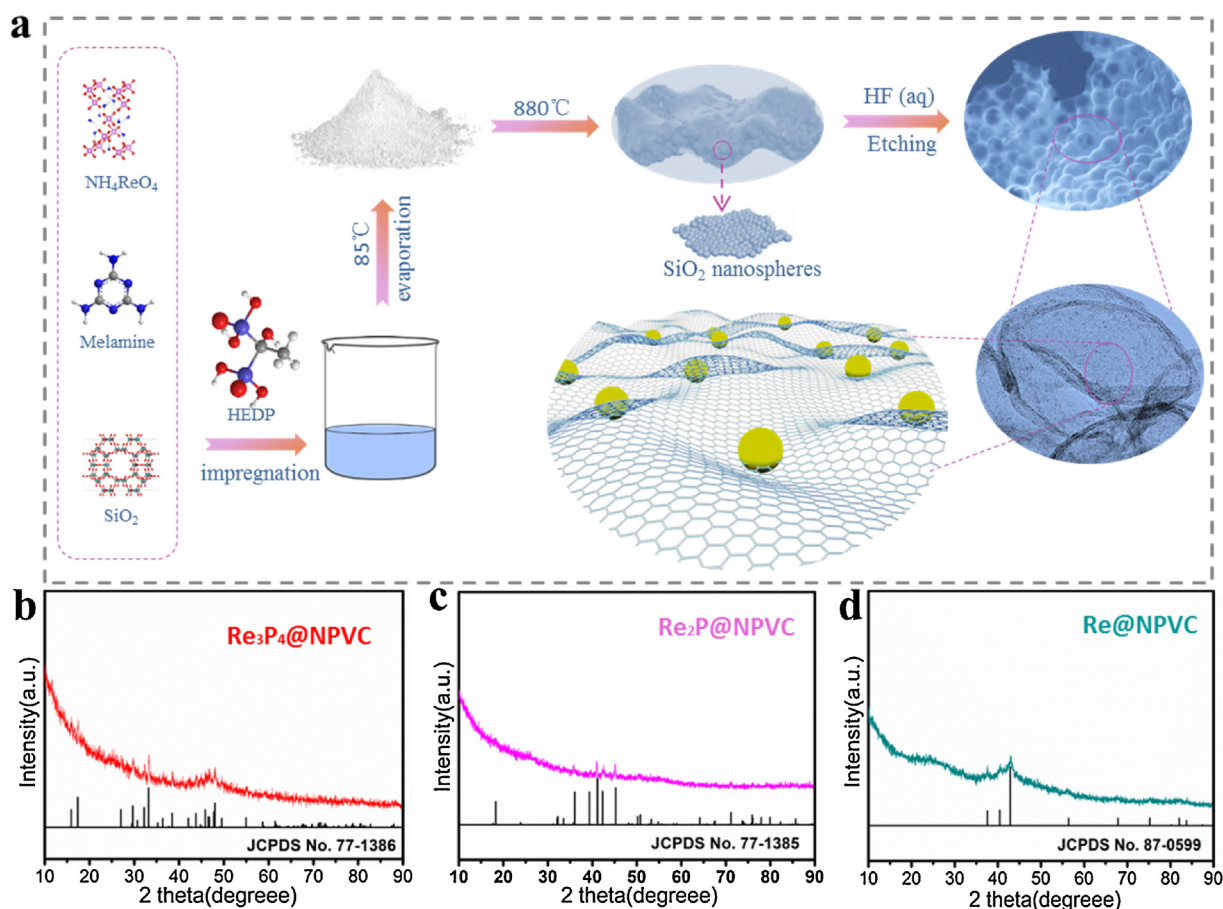
Fig. 1. (a) Schematic illustration for the synthesis procedure and structure of the Re$_3$P$_4$@NPVC and Re$_2$P@NPVC. XRD patterns of (b) Re$_3$P$_4$@NPVC, (c) Re$_2$P@NPVC and (d) Re@NPVC.

splitting electrolysis, a two-electrode configuration was used for electrochemical test in the ceramic diaphram-based alkaline electrolysis cell (1 M KOH), where Re$_3$P$_4$@NPVC or Re$_2$P@NPVC acted as cathode and commercial IrO$_2$ served as anode (the catalyst ink was dropped on the 1 cm^2 nickel foam). To take a comparison, the coupling between commercial Pt/C (cathode) and commercial IrO$_2$ (anode) was evaluated under the same condition.

3. Results and discussion

3.1. Sample synthesis, characterization and electron-transfer properties

Fig. 1a briefly shows the preparation method. First, NH$_4$ReO$_4$, HEDP and melamine molecules uniformly adsorbed on the surface of SiO$_2$ spheres during the heat evaporation process. Then, the high temperature annealing was conducted to convert Re precursors into small-size rhenium phosphides NPs, and simultaneously NPC was formed. More importantly, due to the participation of SiO$_2$ spheres template, these small-size NPs would further auto-assembly anchor in NPC layers around the SiO$_2$ spheres [25]. Finally, the sample can be obtained via etching the SiO$_2$ with HF solution. XRD measurements were carried out to investigate the chemical components. In the XRD pattern (Fig. 1b), the dominant diffraction peaks indexed to the (-111), (-201), (-511), (-202), (400), (201), (311), and (310) planes can affirm the successful synthesis of monoclinic Re$_3$P$_4$ (JCPDS No. 77-1386). Besides, the XRD patterns of Re$_2$P@NPVC (Fig. 1c) and Re@NPVC (Fig. 1d) also confirm their pure crystalline phase structure.

The SEM image and TEM images are shown here to dissect the morphology and construction. As shown in Figs. S1–S3 distinctly exhibits the large-scale vesicular morphology after removal of SiO$_2$

nanospheres (Fig. S4 shows the SEM). These vesicles are interconnected throughout the entire support framework, facilitating the mass transport and accessibility of active sites during the catalytic process. Furthermore, because of the participation of SiO$_2$ nanospheres these vesicles catalysts can manage high-surface-area. Taking Re$_3$P$_4$@NPVC as an example, it possesses a large specific surface area (SSA) (356.0 m^2 g^{-1}), which is much larger than that of Re$_3$P$_4$@NPC without use of SiO$_2$ nanospheres (53.3 m^2 g^{-1}) (Fig. S5). The large SSA can not only contribute to the exposure of active sites, but also increase the intimate contact area with support electrodes, resulting in lower overpotential and rapid ion diffusion, thereby accelerating the catalytic process of HER. [26] Fig. 2a is the magnified TEM images of Re$_3$P$_4$@NPVC, which further demonstrates the vesicular construction. The inset (high-resolution TEM image) in Fig. 2a reveals the lattice fringes with an interplanar value 2.70 Å, corresponding to the (-111) plane of Re$_3$P$_4$. The energy-dispersive X-ray (EDX) mappings (Fig. 2b) demonstrates that the Re, P, C, N elements were homogeneously distributed in the NPVC. The molar ratio of Re to P for Re$_3$P$_4$@NPVC is 0.42 less than 0.75 and for Re$_2$P@NPVC is 1.89 less than 2 (Fig. S6), which further affirms the chemical composition and the doping of P into the support. Similarly the TEM, HRTEM and EDX mapping images of Re$_2$P@NPVC (Fig. 2c and d) can be also obtained. Typically, the lattice fringes crystal with a spacing of 2.49 Å is presented in the HRTEM image, which can be attributed to the (111) lattice plane of Re$_2$P. All above the magnified TEM images maintain that the active NPs are assuredly embedded in the NPVC matrix. The NPs are mainly around 4 nm in size (Fig. S7), which is much smaller than that of Re$_3$P$_4$ bulk (Fig. S8), manifesting the significance of NPVC to astrict the growth of NPs. When the same procedure is conducted without the participation of SiO$_2$ nanospheres, Re$_3$P$_4$ NPs with a size of about 15 nm can be obtained (Fig. S9),
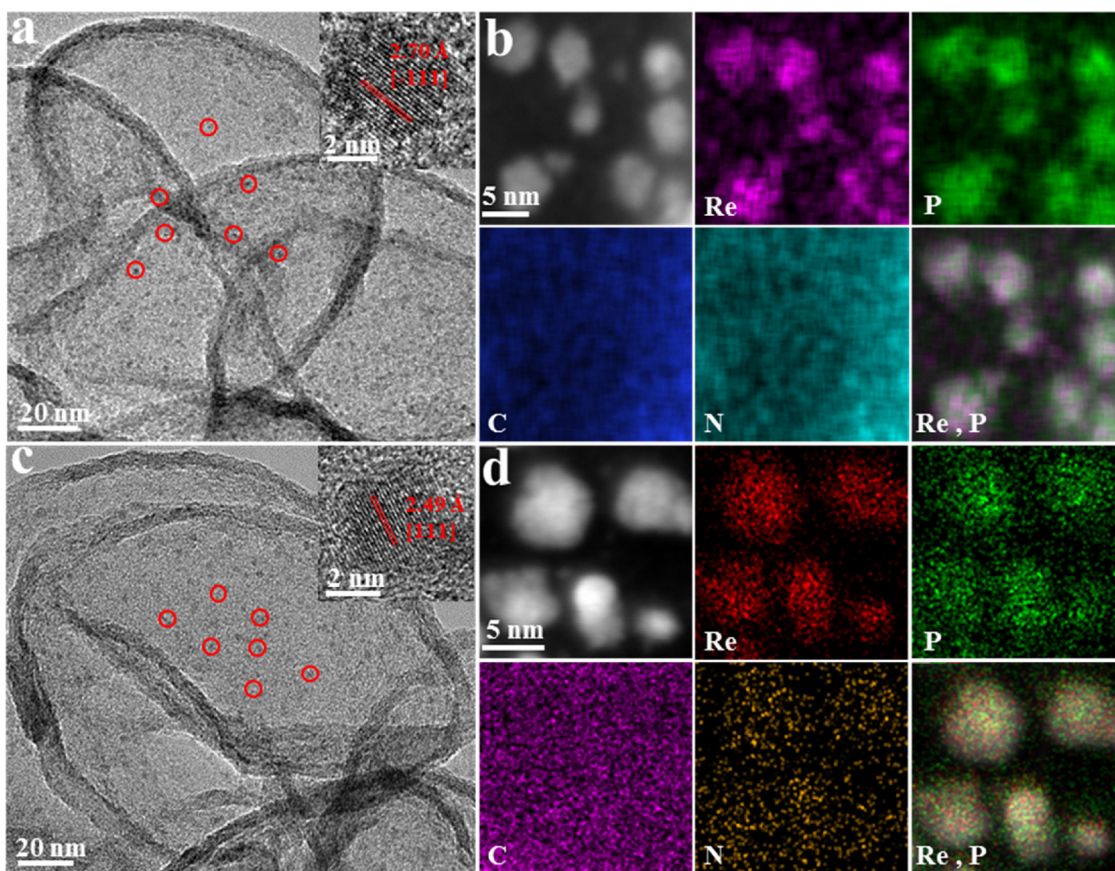
Fig. 2. TEM (a) and (c), EDX elemental mapping (b) and (f) of Re_3P_4@NPVC and Re_2P@NPVC, respectively.

indicating the role of SiO_2 nanospheres to build a thinner NPC framework and further optimize the size of NPs in NPVC. No doubt, the small-size NPs in NPVC can expose substantial active sites for H^+ adsorption reaction [25].

The surface chemical states of Re_3P_4@NPVC, Re_2P@NPVC and Re@NPVC were characterized via XPS technology. Fig. 3a displays the obtained XPS spectrum of the Re 4f regions for Re_3P_4@NPVC, Re_2P@NPVC and Re@NPVC from top to bottom. Correspondingly, the P 2p regions for them are exhibited in Fig. 3b. It's easy to see that the peaks of Re $4f_{7/2}$ regions for Re@NPVC (40.35 eV), Re_2P@NPVC (40.60 eV)

and Re_3P_4@NPVC (40.90 eV) have an obvious positive shift with the increased atomic percentage of P, suggesting that the Re species in rhenium phosphides bear a partial positive charge (δ^+) and the value of δ is in the order: δ (Re) < δ (Re_2P) < δ (Re_3P_4). For the Re-P region in P 2p spectrum, the monoclinic Re_3P_4@NPVC has a slight negative shift, compared with orthorhombic Re_2P@NPVC. These results indicate that the surface electronic state of metal Re has been changed owing to the modification with P. In addition, for exploring the significance of NPVC, Similarly XRD and XPS characteristics of the Re_3P_4 bulk (Figs. S10 and S11) can be also obtained. In contrast with the Re_3P_4@NPVC, it is
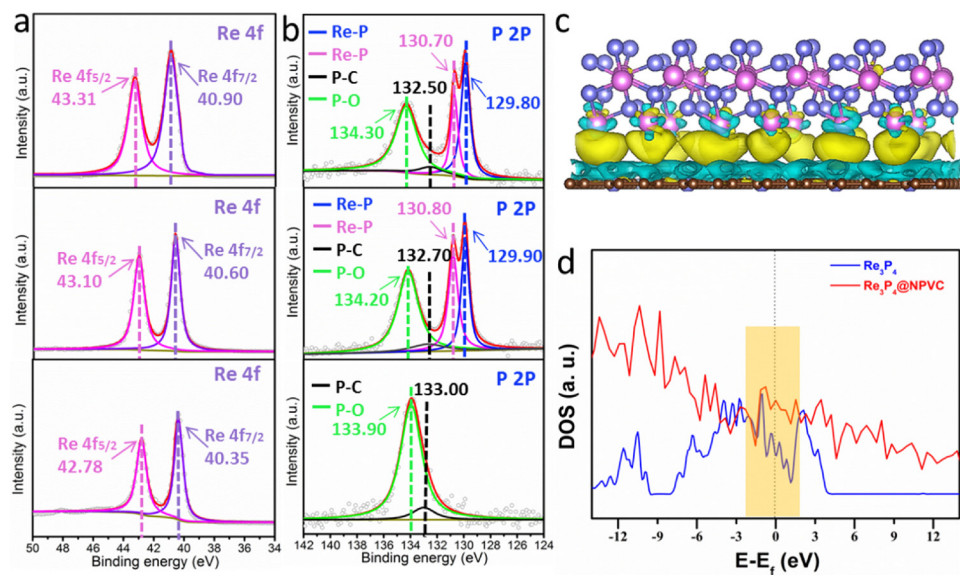

Fig. 3. XPS spectra of (a) Re and (b) P in Re_3P_4@NPVC, Re_2P@NPVC and Re@NPVC from top to bottom. (c) The isosurfaces of local charge density difference of Re_3P_4/NPVC interface. The yellow refers to increased charge distributions, and the cyan shows decreased charge distributions. (d) Calculated density of states for Re_3P_4 bulk and Re_3P_4@NPVC. (For interpretation of the references to colour in this figure legend, the reader is referred to the web version of this article).

worth mentioning that the electron BE of Re $4f_{7/2}$ in Re_3P_4 bulk has an obvious positive shift about 0.35 eV, which can indicate that there is an electron transfer from NPVC to Re_3P_4 NPs. In the HER ($2H^+ + 2e^- \rightleftharpoons H_2$), the enrichment of electrons on the surface of the catalyst can enhance the catalytic activity of the reaction. Hence, H^+ would rather adsorb on the surface of NPs with a large amount of electrons to produce hydrogen [27,28]. To further illustrate this fact, the isosurfaces of local charge density difference of Re_3P_4/NPVC interface was calculated. The calculation result (Fig. 3c) reveals that the charge density in Re_3P_4@NPVC interlayer was reallocated in the form of a transparent electron transfer from NPVC to Re_3P_4 NPs, resulting in an electron-rich region on Re_3P_4 layer. Resulting from electron transfer, there is strong interaction between Re_3P_4 NPs and NPVC, which is of benefit to the high-efficiency HER activity better than that of Re_3P_4 bulk. It also is expected to boost the charge-carrier transport through introducing the NPVC support. As shown in Fig. 3d, the continuous calculated density of states (DOS) near the Fermi level of Re_3P_4 suggests its intrinsic metallic character. Interestingly, the DOS of Re_3P_4@NPVC near the Fermi level is more intense than that of Re_3P_4 bulk. The results show that the electrical property of Re_3P_4, especially the charge-carrier transport and electrical conductivity, can be further enhanced when a NPVC is introduced [29,30]. Furthermore, these peaks for P-C in Fig. 3 suggest that P can be successfully doped into the porous nitrogen doped carbon foam. A series of the Raman spectrum, XPS survey spectrum and electron BE of the C 1s [31] and N 1s [32] regions for Re_3P_4@NPVC (Fig. S12), Re_2P@NPVC (Fig. S13), Re@NPVC (Fig. S14), and NPVC (Fig. S15) were carried out under the same conditions.

3.2. Electrocatalytic activities for HER

Many DFT calculations have demonstrated that the extraordinary electrocatalytic properties of TMPs for HER is intimately linked to the P atoms [18,33]. The electrons of metal atoms are easy to be drawn by P atoms with more electronegativity. In the case of same metal phosphides, increasing the P content may exhibit a better activity towards HER [34]. Accordingly, Re_3P_4@NPVC with more atomic percentage of P may provide more abundant proton-acceptor centers, thus exhibiting superior catalytic activity compared to Re_2P@NPVC and Re@NPVC. Furthermore, the concomitant electron's redistribution between NPs and NPVC can provide a nonresistant path for fast electron transfer through interlayers of NPs and NPVC to expedite the electrocatalytic kinetics for HER. Fig. 4a–c present the polarization curves of the samples in different pH conditions. The required overpotential (η) of Re_3P_4@NPVC is only 40 mV, 70 mV and 61 mV at the current density (10 mA cm^{-2}, j_{10}), respectively. The Tafel slope is closely linked to the reaction kinetics, thus being regarded as one of the great tools in estimating catalytic activity [26]. In order from Fig. 4d to Fig. 4f, the Tafel slope of Re_3P_4@NPVC is 38, 77 and 62 mV dec^{-1} in 0.5 M H_2SO_4 solution, neutral and alkaline media. In addition, the Re_2P@NPVC also shows decent catalytic performance (η_{j10} = 55 mV and Tafel: 43 mV dec^{-1} in 0.5 M H_2SO_4, η_{j10} = 91 mV and Tafel: 123 mV dec^{-1} in 1.0 M PBS, η_{j10} = 74 mV and Tafel: 83 mV dec^{-1} in 1.0 M KOH solution). The catalytic activities of Re_3P_4@NPVC and Re_2P@NPVC at all pH are comparable with most reported phosphide catalysts (FeP-based [23], CoP-based [35,36], NiP$_x$-based, [37–39] MoP-based [40–44], WP-based [45] and Re-based [12,15]) for HER (Table S1), and the former exhibits much better catalytic properties compared to our control samples except Pt/C (Fig. S16). The HER j_0 can be obtained from Tafel plot via using the extrapolation method shown in Fig. S17. The j_0 for Re_2P@NPVC is 0.35 mA cm^{-2}. Note that the j_0 of Re_3P_4@NPVC (0.52 mA cm^{-2}) is even comparable to the commercial Pt/C (0.60 mA cm^{-2}) under the same catalyst loading (0.143 mg cm^{-2}), indicating excellent intrinsic electrocatalytic property. At fixed η of 70 mV versus reversible hydrogen electrode (RHE), the mass activity of Re_3P_4@NPVC is 6.20 mA/μg_{Re} in 0.5 M H_2SO_4, and the Re_2P@NPVC presents 4.31 mA/μg_{Re}, which is much higher than that of Pt/C (2.75 mA/μg_{Pt}). Even in

1.0 M PBS and 1.0 M KOH media, the mass activities of phosphides are still higher than that of Pt/C (Fig. 4g). Hence, it can deduce that the incorporation of P highly boosts the HER activity of Re_3P_4@NPVC and Re_2P@NPVC. Deserved to be mentioned, the loading amount of Re in Re_3P_4@NPVC, Re_2P@NPVC, Re_3P_4@NPC and Re@NPVC for catalytic measurement was maintained at 4.3 μg cm^{-2} calculated by ICP-AES. These results indicate that newly developed Re_3P_4@NPVC can significantly reduce the precious metal loading and meet the cost requirements for future large-scale applications.

To further assess the HER catalytic tolerance of Re_3P_4@NPVC, Re_2P@NPVC and Re@NPVC, their long-term stability was evaluated via the chronopotentiometric analysis at fixed current density (j_{10}). Fig. 4h distinctly suggests that Re_3P_4@NPVC and Re_2P@NPVC can approximately maintain stabilization at least 100 h in 0.5 M H_2SO_4 solution, while the potential of Re@NPVC has an apparent declivity after 45 h. After a long time test in 0.5 M H_2SO_4 solution, the EDX characterization of metal phosphide was implemented again. Figs. S18 and S19 reveal that while the element was homogeneously distributed in the NPVC, the Re/P atomic ratio of Re_3P_4@NPVC and Re_2P@NPVC was changed into 0.40 and 0.81 (Fig. S20), indicating the stabilization of Re_3P_4@NPVC and the partial dissolution of Re_2P. The XRD patterns after stability test of Re_3P_4@NPVC (Fig. S21) and Re_2P@NPVC (Fig. S22) confirm their unchanged crystalline phases. To further characterize the supported entities, some comparative Raman analyses of initial as well as post-reaction specimens were presented, showing a negligible change in the surface of the catalyst (Fig. S23). The long-term stability of Re_3P_4@NPVC in alkaline and neutral media was appraised in this same way. Re_3P_4@NPVC can maintain its stability until 55 h in neutral media (Fig. S24a), but it may be underperforming in alkaline-pH media (Fig. S24b). In addition, to assess the actual results on the performance of rhenium phosphide catalyst in terms of H_2 production vs energy consumption in the experimental electrocatalytic cell, the Faradaic yield is estimated based on the monitored H_2 volume and the theoretical value for HER (Fig. S25). All the results manifest that although hydrogen production of Re_2P@NPVC is not as good as Re_3P_4@NPVC, they all show a 100% Faradaic yield for H_2 evolution. Commendably, the H_2 evolution rate of Re_3P_4@NPVC can reach 1.09 mL h^{-1} and 0.95 mL h^{-1} in 0.5 M H_2SO_4 and 1.0 M KOH (catalyst loading: 0.028 mg).

At the same time, in order to grasp more insights about the electron transfer kinetics of the catalytic process, EIS was also executed [46]. The Nyquist plot (Fig. S26) clearly displays that charge transfer resistant (R_{ct}) of Re_3P_4@PF-NPC is much lower, which is beneficial to convoy the charge for HER, thereby benefitting catalytic reaction. In order to evaluate the active surface areas, the double-layer capacitance (C_{dl}) was tested at the solid-liquid interface [47]. The cyclic voltammogram (Fig. S27) was measured at between 0.0 V and 0.1 V, where these current signals could be only caused by double layer charging [25]. Obviously, comparing the C_{dl} values (Fig. S28) of Re_3P_4@NPVC, Re_2P@NPVC and Re@NPVC, it is easy to deduce that Re_3P_4@NPVC exposes larger electrochemically active surface area (ECSA) [48]. Subsequently, to further evaluate the intrinsic activities of Re_3P_4@NPVC and Re_2P@NPVC, we can calculated their hydrogen turnover frequency (TOF) values based on the j gotten from the polarization curve [49]. TOF is defined as the number of H_2 evolved per second per active site [50]. Based on the ECSA values, we can calculate the TOF values of our catalysts and the details were explicitly described in the supporting information (Fig. S29). Fig. 4i and S30 explicitly show that the Re_3P_4@ NPVC possesses high TOF, which is larger than Re_2P@ NPVC. In order for us to better compare the both, we have sorted out some relevant results (Table S2).

As the we might know, the good activity in half cell does not always guarantee the same performance in the practical feasibility. Given this consideration, the newly developed material (Re_3P_4@NPVC or Re_2P@ NPVC) was utilized as cathode and commercial IrO_2 acted as anode to assemble the ceramic diaphram-based alkaline electrolyzer for overall water splitting. Fig. 5a demonstrates that such IrO_2-Re_3P_4@NPVC and
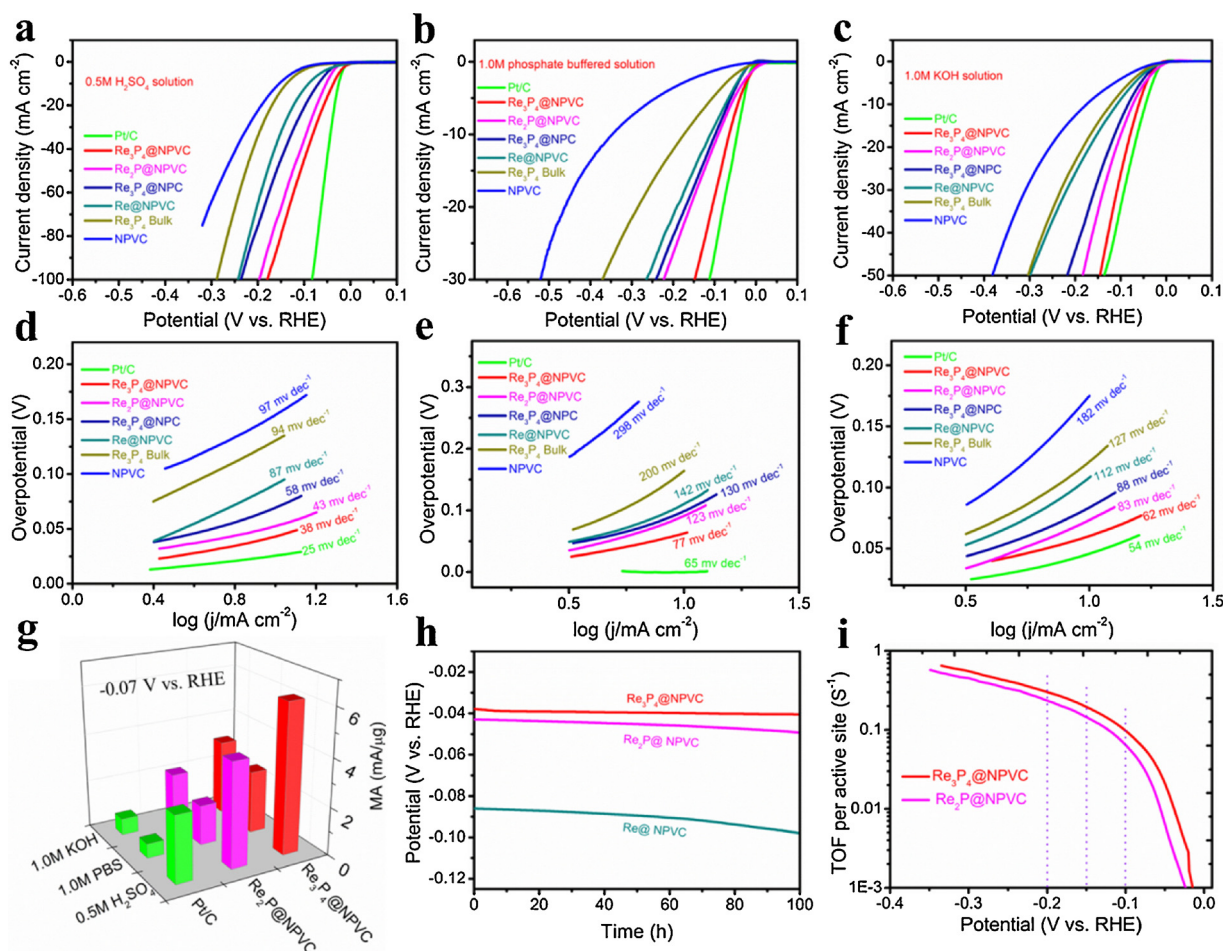
Fig. 4. (a)-(f) Polarization curves of our prepared various catalysts in different pH conditions as well as corresponding Tafel plots. (g) mass activity at −0.07 V vs RHE of Re₃P₄@ NPVC, Re₂P@NPVC and Pt/C. (h) Long-term stability test of Re₃P₄@NPVC, Re₂P@NPVC and Re@NPVC carried out at j_{10} for 100 h in 0.5 M H₂SO₄ solution. (i) TOF curves in 0.5 M H₂SO₄ solution for Re₃P₄@ NPVC and Re₂P@NPVC.
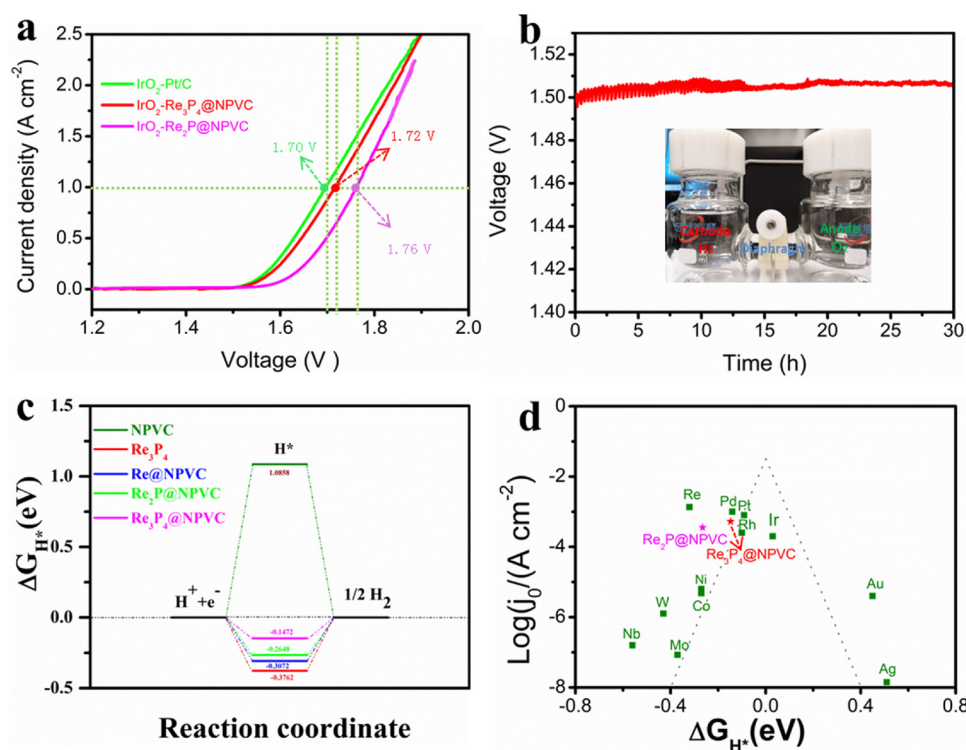

Fig. 5. (a) Polarization curves of IrO2-Re₃P₄@ NPVC, IrO₂-Re₂P@NPVC and commercial IrO2-Pt/C couples in the ceramic diaphram-based alkaline electrolyzer for overall water splitting at 5 mV/s. (b) The long-term stability test for the IrO₂-Re₃P₄@NPVC at current densities of 10 mA cm⁻²; Inset in (b) shows the optical image of the overall water-splitting device. (c) Calculated free-energy diagrams for the HER of our prepared various catalysts. (d) The volcano plot for Re₃P₄@ NPVC (red star), Re₂P@NPVC (purple star), and some familiar metal catalysts (green squares; data refered to ref. [55] and [60]). (For interpretation of the references to colour in this figure legend, the reader is referred to the web version of this article).

IrO_2-Re_2P@NPVC need cell voltage of only 1.50 V and 1.57 V for the current density of 10 mA cm^{-2} (IrO_2-Pt/C, 10 mA cm^{-2} @1.45 V), and reach a current density of 1 A cm^{-2} by 1.72 V and 1.76 V cell voltage (IrO_2-Pt/C, 1 A cm^{-2} @1.7 V). Furthermore, this IrO_2-Re_3P_4@NPVC two-electrode configuration shows a remarkable prolonged stability for at least 30 h without obvious potential degradation (Fig. 5b). In addition, to further correlate the electrochemical results to the actual H_2 evolution rate of catalyst in the two-electrode configuration (IrO_2-Re_3P_4@NPVC), the Faradaic yield is also estimated based on the monitored H_2 volume and the theoretical value for cathodic reaction (Fig. S31). Compared with the half cell, the H_2 evolution rate of Re_3P_4@NPVC (catalyst loading: 0.14 mg) is 4.9 mL h^{-1} by overall-water-splitting cell operating, indicating the laudable H_2 evolution feasibility.

3.3. DFT calculations and volcano plot

In this work, all the theoretical computations were implemented using the generalized gradient approximation (GGA) with the Perdew-Burke-Ernzerh (PBE) [51] within the DFT framework as implemented in Vienna *ab initio* simulation package (VASP) [52]. The project-augmented wave (PAW) method was applied to represent the interaction between ion and electron [53]. Plane wave basis sets were utilized to expand the wave functions of the valence electrons. The energy cutoff for the plane wave basis set was 500 eV [54]. Structural optimizations were performed by minimizing the forces on all the atoms to below 0.03 eV/Å and the energy to below 10^{-5} eV. A 3 × 3x3 Monkhorst-pack grid *k*-points sampling were conducted for the bulk structure optimization, and for the calculation of slab, a 2 × 1x1 Monkhorst-pack grid *k*-points sampling was conducted. More the DFT details were illustrated in the supporting information.

The general belief is that the HER process can be depicted by a three-state diagram (initial state H$^+$ + e$^-$, intermediate state adsorbed H*, and final product ½H$_2$) [13,55,56]. The Gibbs free energy of the intermediate state adsorbed H*, $|\Delta G_{H*}|$, serves as a major estimator of the HER activity, and the most ideal state is that $|\Delta G_{H*}|$ is close to 0 eV [57,58]. The hydrogen release step could be slowed because of the strong hydrogen bonding strength when ΔG_{H*} is lower, whereas the proton/electron transfer step will be endothermal when its ΔG_{H*} is higher [59]. As shown in the optimized structures and free energy diagrams (Figs. S32, 5 c and Table S3), the ΔG_{H*} of Re@NPVC is -0.3072 eV, suggesting that there is a strong adsorption of H*. Re_3P_4@NPVC exhibits the smallest $|\Delta G_{H*}|$ of 0.1471 eV and Re_2P@NPVC is 0.2648 eV, which clearly indicate the better activity of them arising from P atoms. For further comparison, combining the calculated ΔG_{H*} values and we tested HER activities (represented by log j_0 derived from Fig. S17) of the Re_3P_4@NPVC and Re_2P@NPVC, we can establish volcano plot according to Nørskov et al. (Fig. 5d) [55,60]. The property of the catalyst can be assessed by the position of electrocatalytic log j_0 and thermodynamic ΔG_{H*} value relative to the peak of volcano plot (the closer this position is to the peak, the better the performance) [4]. It is clear that the HER activity of the Re_2P@NPVC electrocatalyst transcend some the common non-noble metals. More importantly, newly developed Re_3P_4@NPVC perfectly follows the volcano tendency along with widely collected metal catalysts and displays remarkable HER activity, which can be almost as good as Pt catalyst. Moreover, the DFT calculation results clearly indicate that H* adsorbing on the Re_3P_4 is too strong (-0.3762 eV), whereas on the NPVC (1.0858 eV) is too weak, indicating the unsatisfactory HER activity to the single catalyst [61,62]. Nevertheless, the compounding Re_3P_4 NPs with the NPVC can generate an arbitrated adsorption-desorption behavior ($|\Delta G_{H*}|\rightarrow 0$) to boost the kinetics during overall HER process. Simultaneously, abundant electrons transferred from NPVC layer to catalytically active Re_3P_4 NPs surface can rapidly make the adsorbed H* species easier desorption becoming the final product (H$_2$). It is further manifests that the co-operative effect is critical to facilitate the electrocatalytic activity of heterostructure Re_3P_4@NPVC catalyst.

4. Conclusion

Significantly, this is the first time to obtain novel Re_2P@NPVC and Re_3P_4@NPVC with low metal loading by adopting a new method. These phosphides heterostructures exhibit remarkable electrocatalytic performances for HER at all pH. Among them, Re_3P_4@NPVC is believed to have higher intrinsic activity compared with Re_2P@NPVC due to its higher TOF, with Tafel slopes of 38, 77, and 62 mV dec^{-1} and η_{j10} of 40, 70, and 61 mV in 0.5 M H_2SO_4, 1 M PBS and 1 M KOH and continuous stability above 100 h. Combined experimental observations and theoretical calculations confirm that phosphorus plays a crucial role in arbitrating the robust electrocatalytic properties. In addition, NPVC can efficiently promote the electron-transfer process for the proton reduction. Our synthesis strategy could be extended to design and fabricate other TMPs catalysts with synergistically high-efficiency electrocatalytic properties for HER.

Appendix A. Supplementary data

Supplementary material related to this article can be found, in the online version, at doi:https://doi.org/10.1016/j.apcatb.2019.117851.

References

[1] Y. Shi, B. Zhang, Correction: recent advances in transition metal phosphide nanomaterials: synthesis and applications in hydrogen evolution reaction, Chem. Soc. Rev. 45 (2016), https://doi.org/10.1039/C6CS90013E 1781-1781.

[2] H. Yan, C. Tian, L. Wang, A. Wu, M. Meng, L. Zhao, H. Fu, Phosphorus-modified tungsten Nitride/Reduced graphene oxide as a high-performance, Non-Noble-Metal Electrocatalyst for the hydrogen evolution reaction, Angew. Chem. 127 (2015) 6423–6427, https://doi.org/10.1002/ange.201501419.

[3] C. Tang, L. Gan, R. Zhang, W. Lu, X. Jiang, A.M. Asiri, X. Sun, J. Wang, L. Chen, Ternary FexCo1–xP nanowire array as a robust hydrogen evolution reaction electrocatalyst with Pt-like activity: experimental and theoretical insight, Nano Lett. 16 (2016) 6617, https://doi.org/10.1021/acs.nanolett.6b03332.

[4] Y. Zheng, Y. Jiao, Y. Zhu, L.H. Li, Y. Han, Y. Chen, A. Du, M. Jaroniec, S.Z. Qiao, Hydrogen evolution by a metal-free electrocatalyst, Nat. Commun. 5 (2014) 4783, https://doi.org/10.1038/ncomms4783.

[5] J. Liu, Q. Ma, Z. Huang, G. Liu, H. Zhang, Recent progress in graphene-based noble-metal nanocomposites for electrocatalytic applications, Adv. Mater. (2018) e1800696, , https://doi.org/10.1002/adma.201800696.

[6] J. Hamalainen, K. Mizohata, K. Meinander, M. Mattinen, M. Vehkamaki, J. Raisanen, M. Ritala, M. Leskela, Rhenium metal and rhenium nitride thin films grown by atomic layer deposition, Angew. Chem. 57 (2018) 14538–14542, https://doi.org/10.1002/anie.201806985.

[7] R. Kojima, K.I. Aika, Rhenium containing binary catalysts for ammonia synthesis, Appl.Catal. A 209 (2001) 317–325, https://doi.org/10.1016/S0926-860X(00)00764-X.

[8] R. Kojima, H. Enomoto, M. Muhler, K.I. Aika, Cesium-promoted rhenium catalysts supported on alumina for ammonia synthesis, Appl. Catal. A Gen. 246 (2003) 311–322, https://doi.org/10.1016/S0926-860X(03)00062-0.

[9] E. Muñoz, R. Schrebler, R. Henríquez, C. Heyser, P.A. Verdugo, R. Marotti, Photoelectrochemical reduction of nitrate on p-Si coated with metallic Re thin films, Thin Solid Films 518 (2009) 138–146, https://doi.org/10.1016/j.tsf.2009.06.010.

[10] J. Räty, T.A. Pakkanen, Controlled gas-phase preparation and HDS activity of Re 2 (CO) 10 alumina catalysts, Catal. Lett. 65 (2000) 175–180, https://doi.org/10.1023/A:1019006413873.

[11] N. Escalona, M. Yates, P. Ávila, A.L. Agudo, J. Ojeda, Effect of Re loading on the structure, activity and selectivity of Re/C catalysts in hydrodenitrogenation and hydrodesulphurisation of gas oil, Appl. Catal. A Gen. 240 (2003) 151–160, https://

doi.org/10.1016/S0926-860X(02)00430-1.

[12] Z. Lai, A. Chaturvedi, Y. Wang, T.H. Tran, X. Liu, C. Tan, Z. Luo, B. Chen, Y. Huang, G.H. Nam, Z. Zhang, Y. Chen, Z. Hu, B. Li, S. Xi, Q. Zhang, Y. Zong, L. Gu, C. Kloc, Y. Du, H. Zhang, Preparation of 1T'-phase ReS2 xSe2(1- x) (x = 0-1) nanodots for highly efficient electrocatalytic hydrogen evolution reaction, J. Am. Chem. Soc. 140 (2018) 8563–8568, https://doi.org/10.1021/jacs.8b04513.

[13] J.K. Nørskov, T. Bligaard, A. Logadottir, J.R. Kitchin, J.G. Chen, S. Pandelov, U. Stimming, Trends in the exchange current for hydrogen evolution, J. Electrochem. Soc. 152 (2005) J23–J26, https://doi.org/10.1149/1.1856988.

[14] M.H. MILES, Evaluation of electrocatalysts for water electrolysis in alkaline solutions, J. Electroanal. Chem. 60 (1975) 89–96, https://doi.org/10.1016/S0022-0728(75)80205-1.

[15] Y. Zhou, E. Song, J. Zhou, J. Lin, R. Ma, Y. Wang, W. Qiu, R. Shen, K. Suenaga, Q. Liu, Auto-optimizing Hydrogen Evolution Catalytic Activity of ReS2 through Intrinsic Charge Engineering, ACS Nano 8 (2018) 4627–4632, https://doi.org/10.1021/acsnano.8b00693.

[16] E.J. Popczun, J.R. Mckone, C.G. Read, A.J. Biacchi, A.M. Wiltrout, N.S. Lewis, R.E. Schaak, Nanostructured nickel phosphide as an electrocatalyst for the hydrogen evolution reaction, J. Am. Chem. Soc. 135 (2013) 9267–9270, https://doi.org/10.1021/ja403440e.

[17] S. Carenco, D. Portehault, C. Boissière, N. Mézailles, C. Sanchez, Nanoscaled metal borides and phosphides: recent developments and perspectives, Chem. Rev. 113 (2013) 7981–8065, https://doi.org/10.1021/cr400020d.

[18] P.L. and, J.A. Rodriguez, Catalysts for hydrogen evolution from the [NiFe] hydrogenase to the Ni2P(001) surface: the importance of ensemble effect, J. Am. Chem. Soc. 127 (2005) 14871–14878, https://doi.org/10.1021/ja0540019.

[19] M. Sun, H. Liu, J. Qu, J. Li, Earth-rich transition metal phosphide for energy conversion and storage, Adv. Energy Mater. 6 (2016) 1600087, , https://doi.org/10.1002/aenm.201600087.

[20] S. Pu, M. Chen, Y. Chen, W. Zhang, H. Soliman, A. Qu, Q. Liu, X. Tang, N. Huang, G. Wan, Zirconium ions integrated in 1-hydroxyethylidene-1,1-diphosphonic acid (HEDP) as a metalorganic-like complex coating on biodegradable magnesium for corrosion control, Corros. Sci. 144 (2018) 277–287, https://doi.org/10.1016/j.corsci.2018.09.003.

[21] P. Yin, Z. Wang, R. Qu, X. Liu, J. Zhang, Q. Xu, Biosorption of heavy metal ions onto agricultural residues buckwheat hulls functionalized with 1-hydroxylethylidenediphosphonic acid, J. Agric. Food Chem. 60 (2012) 11664, https://doi.org/10.1021/jf303565d.

[22] Z. Pu, I.S. Amiinu, Z. Kou, W. Li, S. Mu, RuP2-based catalysts with platinum-like activity and higher durability for hydrogen evolution reaction at all pH values, Angew. Chem. 56 (2017) 11559–11564, https://doi.org/10.1002/anie.201704911.

[23] Z. Pu, I.S. Amiinu, C. Zhang, M. Wang, Z. Kou, S. Mu, Phytic acid-derivative transition metal phosphides encapsulated in N,P-codoped carbon: an efficient and durable hydrogen evolution electrocatalyst in a wide pH range, Nanoscale 9 (2017) 3555–3560, https://doi.org/10.1039/c6nr09883e.

[24] R. Koole, M.M.V. Schooneveld, J. Hilhorst, C.D.M. Donegá, D.C.'. Hart, A.V. Blaaderen, D. Vanmaekelbergh, A. Meijerink, On the incorporation mechanism of hydrophobic quantum dots in silica spheres by a reverse microemulsion method, Chem. Mater. 20 (2008) 2503–2512, https://doi.org/10.1021/cm703348y.

[25] H. Yan, C. Tian, L. Wang, A. Wu, M. Meng, L. Zhao, H. Fu, Phosphorus-modified tungsten nitride/reduced graphene oxide as a high-performance, non-noble-metal electrocatalyst for the hydrogen evolution reaction, Angew. Chem. Int. Ed. Engl. 54 (2015) 6325–6329, https://doi.org/10.1002/anie.201501419.

[26] C. Yin, J. Deng, L. Fang, Y. Wang, X. Yang, X. Gu, Y. Wang, Hierarchical urchin-like peapoded core-shell-structured NiCo2@Ni1/3Co2/3S2@C catalyst with synergistically high-efficiency electrocatalytic properties toward hydrogen evolution reaction, J. Catal. 365 (2018) 351–358, https://doi.org/10.1016/j.jcat.2018.07.020.

[27] B. Zhang, J. Liu, J. Wang, Y. Ruan, X. Ji, K. Xu, C. Chen, H. Wan, L. Miao, J. Jiang, Interface engineering: the Ni(OH) 2 /MoS 2 heterostructure for highly efficient alkaline hydrogen evolution, Nano Energy 37 (2017) 74–80, https://doi.org/10.1016/j.nanoen.2017.05.011.

[28] L. Chen, J. Zhang, X. Ren, R. Ge, W. Teng, X. Sun, X. Li, A Ni(OH)2-CoS2 hybrid nanowire array: a superior non-noble-metal catalyst toward the hydrogen evolution reaction in alkaline media, Nanoscale 9 (2017) 16632–16637, https://doi.org/10.1039/c7nr06001g.

[29] K. Xu, P. Chen, X. Li, Y. Tong, H. Ding, X. Wu, W. Chu, Z. Peng, C. Wu, Y. Xie, Metallic nickel nitride nanosheets realizing enhanced electrochemical water oxidation, J. Am. Chem. Soc. 137 (2015) 4119–4125, https://doi.org/10.1021/ja5119495.

[30] X. Jia, Y. Zhao, G. Chen, L. Shang, R. Shi, X. Kang, G.I.N. Waterhouse, L.-Z. Wu, C.-H. Tung, T. Zhang, Ni3FeN Nanoparticles Derived from Ultrathin NiFe-Layered Double Hydroxide Nanosheets: An Efficient Overall Water Splitting Electrocatalyst, Adv. Energy Mater. 6 (2016) 1502585, , https://doi.org/10.1002/aenm.201502585.

[31] Z. Lin, G. Waller, Y. Liu, M. Liu, C.P. Wong, Facile synthesis of nitrogen-doped graphene via pyrolysis of graphene oxide and urea, and its electrocatalytic activity toward the oxygen-reduction reaction, Adv. Energy Mater. 2 (2012) 884–888, https://doi.org/10.1002/aenm.201200038.

[32] Z. Pu, I.S. Amiinu, X. Liu, M. Wang, S. Mu, Ultrastable nitrogen-doped carbon encapsulating molybdenum phosphide nanoparticles as highly efficient electrocatalyst for hydrogen generation, Nanoscale 8 (2016) 17256–17261, https://doi.org/10.1039/C6NR05564H.

[33] P. Xiao, M.A. Sk, L. Thia, X. Ge, R.J. Lim, J.Y. Wang, K.H. Lim, X. Wang, Molybdenum phosphide as an efficient electrocatalyst for the hydrogen evolution reaction, Energy Environ, Sci. 7 (2014) 2624–2629, https://doi.org/10.1039/C4EE00957F.

[34] Y. Shi, B. Zhang, Recent advances in transition metal phosphide nanomaterials: synthesis and applications in hydrogen evolution reaction, Chem. Soc. Rev. 45 (2016) 1529–1541, https://doi.org/10.1039/c5cs00434a.

[35] J. Ma, M. Wang, G. Lei, G. Zhang, F. Zhang, W. Peng, X. Fan, Y. Li, Polyaniline derived N-Doped carbon-coated cobalt phosphide nanoparticles deposited on N-Doped graphene as an efficient electrocatalyst for hydrogen evolution reaction, Small 14 (2017) 1702895, , https://doi.org/10.1002/smll.201702895.

[36] Z.H. Xue, S. Hui, Q.Y. Yu, Z. Bing, H.H. Wang, X.H. Li, J.S. Chen, Janus Co/CoP nanoparticles as efficient mott-schottky electrocatalysts for overall water splitting in wide pH range, Adv. Energy Mater. 7 (2017) 1602355, , https://doi.org/10.1002/aenm.201602355.

[37] Z. Huang, Z. Chen, Z. Chen, C. Lv, H. Meng, C. Zhang, Ni12P5 nanoparticles as an efficient catalyst for hydrogen generation via electrolysis and photoelectrolysis, ACS Nano 8 (2014) 8121–8129, https://doi.org/10.1021/nn5022204.

[38] Y. Pan, Y. Liu, J. Zhao, K. Yang, J. Liang, D. Liu, W. Hu, D. Liu, Y. Liu, C. Liu, Monodispersed nickel phosphide nanocrystals with different phases: synthesis, characterization and electrocatalytic properties for hydrogen evolution, J. Mater. Chem. A Mater. Energy Sustain. 3 (2014) 1656–1665, https://doi.org/10.1039/c4ta04867a.

[39] L. Feng, H. Vrubel, M. Bensimon, X. Hu, Easily-prepared dinickel phosphide (Ni2P) nanoparticles as an efficient and robust electrocatalyst for hydrogen evolution, Phys. Chem. Chem. Phys. 16 (2014) 5917–5921, https://doi.org/10.1039/c4cp00482e.

[40] Y. Huang, X. Song, J. Deng, C. Zha, W. Huang, Y. Wu, Y. Li, Ultra-dispersed molybdenum phosphide and phosphosulfide nanoparticles on hierarchical carbonaceous scaffolds for hydrogen evolution electrocatalysis, Appl. Catal. BEnviron. 245 (2019) 656–661, https://doi.org/10.1016/j.apcatb.2019.01.034.

[41] J.S. Li, J.Q. Sha, B. Du, B. Tang, Highly efficient hydrogen evolution electrocatalysts based on coupled molybdenum phosphide and reduced graphene oxide derived from MOFs, Chem. Commun. 53 (2017) 12576–12579, https://doi.org/10.1039/C7CC06660K.

[42] X. Liu, L. Zhang, M. Li, X. Hu, Tandem MoP nanocrystals with rich grain boundaries for efficient electrocatalytic hydrogen evolution, Chem. Commun. 54 (2018) 2502–2505, https://doi.org/10.1039/C7CC09137K.

[43] Z. Wu, J. Wang, R. Liu, K. Xia, C. Xuan, J. Guo, W. Lei, D. Wang, Facile preparation of carbon sphere supported molybdenum compounds (P, C and S) as hydrogen evolution electrocatalysts in acid and alkaline electrolytes, Nano Energy 32 (2017) 511–519, https://doi.org/10.1016/j.nanoen.2017.01.014.

[44] X. Zhang, X.L. Yu, L.J. Zhang, F. Zhou, Y.Y. Liang, R.H. Wang, Molybdenum Phosphide/Carbon nanotube hybrids as pH-Universal electrocatalysts for hydrogen evolution reaction, Adv. Funct. Mater. 28 (2018) 1706523, , https://doi.org/10.1002/adfm.201706523.

[45] Z. Pu, Y. Xue, I.S. Amiinu, Z. Tu, X. Liu, W. Li, S. Mu, Ultrasmall tungsten phosphide nanoparticles embedded in nitrogen- doped carbon as a highly active and stable hydrogen- evolution electrocatalyst, J. Mater. Chem. A 4 (2016), https://doi.org/10.1039/c6ta05165k 15249-15249.

[46] Y. Yin, J. Han, Y. Zhang, X. Zhang, P. Xu, Q. Yuan, L. Samad, X. Wang, Y. Wang, Z. Zhang, Contributions of phase, sulfur vacancies, and edges to the hydrogen evolution reaction catalytic activity of porous molybdenum disulfide nanosheets, J. Am. Chem. Soc. 138 (2016) 7965–7972, https://doi.org/10.1021/jacs.6b03741.

[47] S. Trasatti, O.A. Petrii, Real surface area measurements in electrochemistry, Pure Appl. Chem. 63 (1991) 711–734, https://doi.org/10.1351/pac199163050711.

[48] S. Carenco, D. Portehault, C. Boissière, N. Mézailles, C. Sanchez, Nanoscaled metal borides and phosphides: recent developments and perspectives, Chem. Rev. 113 (2013) 7981, https://doi.org/10.1021/cr400020d.

[49] K. Jakob, T.F. Jaramillo, Molybdenum phosphosulfide: an active, acid-stable, earthabundant catalyst for the hydrogen evolution reaction, Angew. Chem. 126 (2015) 14661–14665, https://doi.org/10.1002/anie.201408222.

[50] Y. Zheng, Y. Jiao, Y. Zhu, L.H. Li, Y. Han, Y. Chen, M. Jaroniec, S.Z. Qiao, High electrocatalytic hydrogen evolution activity of an anomalous ruthenium catalyst, J. Am. Chem. Soc. 138 (2016) 16174–16181, https://doi.org/10.1021/jacs.6b11291.

[51] J.P. Perdew, K. Burke, M. Ernzerhof, Generalized gradient approximation made simple, Phys. Rev. Lett. 77 (1996) 3865–3868, https://doi.org/10.1103/PhysRevLett.77.3865.

[52] G. Kresse, D. Joubert, From ultrasoft pseudopotentials to the projector augmented-wave method, Phys. Rev. B 59 (1999) 1758–1775, https://doi.org/10.1103/PhysRevB.59.1758.

[53] X. Xie, Y. Li, Z.Q. Liu, M. Haruta, W. Shen, Low-temperature oxidation of CO catalysed by Co(3)O(4) nanorods, Nature 458 (2009) 746–749, https://doi.org/10.1038/nature07877.

[54] X. Gu, J.-l. Liu, J.-h. Yang, H.-j. Xiang, X.-g. Gong, Y.-y. Xia, First-principles study of H+ intercalation in layer-structured LiCoO2, J. Phys. Chem. B 115 (2011) 12672–12676, https://doi.org/10.1021/jp202846p.

[55] J.K. Norskov, T. Bligaard, J. Rossmeisl, C.H. Christensen, Towards the computational design of solid catalysts, Nat. Chem. 1 (2009) 37–46, https://doi.org/10.1038/nchem.121.

[56] J. Greeley, T.F. Jaramillo, J. Bonde, I.B. Chorkendorff, J.K. Nørskov, Computational high-throughput screening of electrocatalytic materials for hydrogen evolution, Nat. Mater. 5 (2006) 909–913, https://doi.org/10.1038/nmat1752.

[57] B. Hinnemann, P.G. Moses, J. Bonde, K.P. Joergensen, J.H. Nielsen, S. Horch, I. Chorkendorff, J.K. Noerskov, Biomimetic hydrogen evolution: MoS 2 nanoparticles as catalyst for hydrogen evolution, J. Am. Chem. Soc. 36 (2005) 5308–5309, https://doi.org/10.1021/ja0504690.

[58] E. Skúlason, V. Tripkovic, M.E. Björketun, S. Gudmundsdóttir, G. Karlberg, J. Rossmeisl, T. Bligaard, H. Jónsson, J.K. Nørskov, Modeling the electrochemical hydrogen oxidation and evolution reactions on the basis of density functional

theory calculations, J. Phys. Chem. C 114 (2010) 18182–18197, https://doi.org/10.1021/jp1048887.

[59] H. Duan, D. Li, Y. Tang, Y. He, S. Ji, R. Wang, H. Lv, P.P. Lopes, A.P. Paulikas, H. Li, High-performance Rh2P electrocatalyst for efficient water splitting, J. Am. Chem. Soc. 139 (2017) 5494–5502, https://doi.org/10.1021/jacs.7b01376.

[60] J. Greeley, T.F. Jaramillo, J. Bonde, I.B. Chorkendorff, J.K. Norskov, Computational high-throughput screening of electrocatalytic materials for hydrogen evolution, Nat. Mater. 5 (2006) 909–913, https://doi.org/10.1038/nmat1752.

[61] Z. Wang, Z. Liu, G. Du, A.M. Asiri, L. Wang, X. Li, H. Wang, X. Sun, L. Chen, Q. Zhang, Ultrafine PtO2 nanoparticles coupled with a Co(OH)F nanowire array for enhanced hydrogen evolution, Chem. Commun. 54 (2018) 810–813, https://doi.org/10.1039/c7cc08870a.

[62] L.L. Feng, G. Yu, Y. Wu, G.D. Li, H. Li, Y. Sun, T. Asefa, W. Chen, X. Zou, High-index faceted Ni3S2 nanosheet arrays as highly active and ultrastable electrocatalysts for water splitting, J. Am. Chem. Soc. 137 (2015) 14023–14026, https://doi.org/10.1021/jacs.5b08186.